The Journal of Immunology

Kinetics of MHC-CD8 Interaction at the T Cell Membrane

Jun Huang, Lindsay J. Edwards, Brian D. Evavold and Cheng Zhu

J Immunol 2007; 179:7653-7662; ;
doi: 10.4049/jimmunol.179.11.7653
http://www.jimmunol.org/content/179/11/7653

The Journal of Immunology is published twice each month by
The American Association of Immunologists, Inc.,
1451 Rockville Pike, Suite 650, Rockville, MD 20852

Print ISSN: 0022-1767 Online ISSN: 1550-6606.

Kinetics of MHC-CD8 Interaction at the T Cell Membrane[1]

Jun Huang,* Lindsay J. Edwards,† Brian D. Evavold,† and Cheng Zhu[2]*‡

CD8 plays an important role in facilitating TCR-MHC interaction, promoting Ag recognition, and initiating T cell activation. MHC-CD8 binding kinetics have been measured in three dimensions by surface plasmon resonance technique using purified molecules. However, CD8 is a membrane-anchored, signaling kinase-linked, and TCR-associated molecule whose function depends on the cell membrane environment. Purified molecules lack their linkage to the membrane, which precludes interactions with other structures of the cell as well as signaling. Furthermore, three-dimensional binding in the fluid phase is biologically and physically distinct from two-dimensional binding across apposing cell membranes. As a first step toward characterizing the molecular interactions between T cells and APCs, we used a micropipette adhesion frequency assay to measure the adhesion kinetics of single mouse T cells interacting with single human RBCs coated with MHC. Using anti-TCR mAb we isolated and characterized the specific two-dimensional MHC-CD8 binding from the trimolecular TCR-MHC-CD8 interaction. The TCR-independent MHC-CD8 interaction has a very low affinity that depends on the MHC alleles, but not on the peptide complexed to the MHC and whether CD8 is an $\alpha\alpha$ homodimer or an $\alpha\beta$ heterodimer. Surprisingly, MHC-CD8 binding affinity varies with T cells from different TCR transgenic mice and these affinity differences were abolished by treatment with cholesterol oxidase to disrupt membrane rafts. These data highlight the relevance and importance of two-dimensional analysis of T cells and APCs and indicate that membrane rafts play an important role in modulating the affinity of cell-cell interactions. *The Journal of Immunology,* **2007, 179: 7653–7662.**

The CD8 glycoprotein was initially discovered as a cell surface marker distinguishing CTLs from helper T cells in mice (1) and, along with TCR and CD3, is part of the surface molecular assembly involved in Ag recognition (2). As a coreceptor, CD8 associates with the Src family kinase $p56^{lck}$ (Lck),[3] which can phosphorylate CD3ζ and initiate T cell activation. CD8 also serves as an adhesion molecule to bind MHC to promote and stabilize the interaction of MHC with TCR (1, 3–9), which recognizes the specific peptide complexed with MHC (pMHC) (10, 11). This dual function provides an opportunity, but does not necessarily set a requirement, for TCR-MHC and MHC-CD8 interactions to affect each other. However, it is controversial whether coreceptor CD8 and TCR bind pMHC cooperatively or independently (3, 5, 7, 12–15).

On the T cell surface, CD8 is expressed as either a homodimer CD8$\alpha\alpha$ or a heterodimer CD8$\alpha\beta$ linked by a disulfide bond (1, 4, 12). The α- and β-chains are encoded by two closely related genes (16) and share ~20% amino acid sequence homology (1). CD8$\alpha\beta$ is expressed primarily on peripheral $\alpha\beta$ T cells whereas CD8$\alpha\alpha$ is expressed broadly on $\alpha\beta$ T cells, $\gamma\delta$ T cells, NK cells, and dendritic cells (1, 4, 17). CD8$\alpha\beta$ has been shown to be a more potent coreceptor than CD8$\alpha\alpha$ in helping the TCR recognize Ag (1, 4, 18–20), but the reason for this is unclear (1, 4, 16, 17, 19, 20). One possibility is that CD8$\alpha\beta$ may have a higher affinity for MHC than CD8$\alpha\alpha$. Only cell surface CD8$\alpha\beta$, but not CD8$\alpha\alpha$ or soluble CD8$\alpha\beta$, has been found to significantly increase the avidity of TCR-MHC binding (4). Furthermore, inconsistent results have been obtained using cell adhesion (21), surface plasmon resonance (SPR) (22–25), and MHC tetramer staining assays (16).

During thymocyte development, positive and negative selection ensures generation of a repertoire of self-MHC-restricted and self-peptide-tolerant T cells; the trimolecular interaction of TCR, pMHC, and CD8 plays a critical role in determining the fate of a developing thymocyte. The kinetic properties of CD8 binding to polymorphic MHC may serve as determinants in the selection process (26–28), just like the kinetic properties of TCR binding to pMHC are determinants of T cell recognition (10).

Although several studies have used SPR to measure MHC-CD8 binding kinetics, these measurements may not account for all interaction characteristics of CD8 on the T cell membrane. The cell membrane provides an important environment for molecular assembly and interactions (29). Many cell surface molecules have to be assembled or linked to other membrane molecules/structures to carry out their functions fully. For example, TCR$\alpha\beta$ is complexed with CD3 signaling module (CD3$\delta\varepsilon$, CD3$\gamma\varepsilon$, CD3$\zeta\zeta$) via its transmembrane domain (30). For the CD8 molecule in particular, the larger α- (than β-) chain connects CD8 to the signaling kinase Lck through its cytoplasmic domain (1, 4). The β-chain promotes constitutive association of CD8 with TCR/CD3 via its shorter cytoplasmic tail (4) and mediates CD8 partitioning in membrane rafts (4, 16). Recombinant molecules purified for SPR studies lack the linkage to the cell membrane, which precludes their interactions with other molecules on cell surface and intracellular structures such as signaling molecules that may regulate binding. For this reason, interactions between molecules respectively anchored on two apposing cell membranes can be biologically different from and more relevant to molecular recognition than those in solution using purified molecules.

*Coulter Department of Biomedical Engineering, and ‡Woodruff School of Mechanical Engineering, Georgia Institute of Technology, Atlanta, Georgia 30332; and †Department of Microbiology and Immunology, Emory University, Atlanta, GA 30322

Received for publication May 15, 2007. Accepted for publication September 17, 2007.

The costs of publication of this article were defrayed in part by the payment of page charges. This article must therefore be hereby marked *advertisement* in accordance with 18 U.S.C. Section 1734 solely to indicate this fact.

[1] This work was supported by National Institutes of Health Grants AI38282 (to C.Z.) and AI56017 (to B.D.E.).

[2] Address correspondence and reprint requests to Dr. Cheng Zhu, Coulter Department of Biomedical Engineering, Georgia Institute of Technology, 315 Ferst Drive, Atlanta, GA 30332. E-mail address: cheng.zhu@bme.gatech.edu

[3] Abbreviations used in this paper: Lck, Src kinase $p56^{lck}$; EAS45, experimental additive solutions 45; pMHC, peptide MHC; SPR, surface plasmon resonance; 2D, two dimension(al); 3D, three dimension(al).

Indeed, the former is referred to as two-dimensional (2D) interaction and the latter as three-dimensional (3D) interaction, which are physically distinct (31). The equilibrium dissociation constant (K_d) is expressed as the number of molecules per unit space based on the mass action law. In the fluid phase, molecules are brought together by diffusion and/or flow in a volume, the concentration has a unit of M, and the 3D binding affinity is measured in M^{-1}. By comparison, molecules anchored on the cell membrane diffuse along a surface, their site density has a unit of μm^{-2}, and the 2D binding affinity is measured in μm^2. More importantly, the two interacting cells have to be brought together because membranes separated by a distance greater than the molecular size would physically preclude binding. It has been demonstrated that the molecular length and orientation (32) as well as cell surface microtopology and stiffness can significantly affect 2D (but not 3D) affinity (33, 34). Although the reverse-rate k_r has the same unit (in s^{-1}) for 2D and 3D interaction, only in the 2D (but not 3D) case can k_r be regulated by force applied to the molecular bonds—they would be disrupted by the separation of the cells (31).

As a first step toward characterizing the 2D molecular interactions between T cells and APCs, we used a micropipette adhesion frequency assay (35) to measure the TCR-independent 2D kinetics of CD8 on the T cell membrane interacting with MHC coated on the surface of RBCs. Consistent with published SPR results, the 2D MHC-CD8 interaction was of very low affinity and depend on the MHC alleles but not on the peptide with which the MHC was complexed. The MHC-CD8 interaction was also indifferent to whether CD8 was composed of an $\alpha\alpha$ homodimer or an $\alpha\beta$ heterodimer. Surprisingly, the 2D affinity for the same MHC varied with T cells from different TCR transgenic mice on which the CD8 was expressed. These affinity differences were abolished by treatment with cholesterol oxidase to disrupt membrane rafts, which reduced MHC-CD8 binding affinity differentially in different T cells. These findings highlight the difference between 2D and 3D binding and emphasize the importance of directly measuring molecular interactions between T cells and APCs with 2D methods.

Materials and Methods

Mice and cell preparation

OTI transgenic mice expressing H-2K^b MHC-restricted OTI TCR specific for an OVA epitope (aa 257–264) of OVA (10, 36, 37), P14 transgenic mice expressing H-2D^b MHC-restricted P14 TCR specific for a gp33 epitope (aa 33–41) of lymphocytic choriomeningitis virus (38) and F5 transgenic mice expressing H-2D^b MHC-restricted F5 TCR specific for an epitope (aa 366–374) of influenza nucleoprotein (39) were housed in the Emory University Department of Animal Resources facility according to a protocol approved by the Institutional Animal Care and Use Committee of Emory University. Naive OTI, P14, and F5 T cells from transgenic mice were purified using MACS according to the manufacturer's instructions (Miltenyi Biotec). In brief, a single cell suspension of splenocytes was incubated with anti-CD8 positive selection magnetic beads. Cells were washed, run through a magnetic column, and eluted. Purified T cells were washed and stored at 4°C for use up to 2 days.

Human RBCs were isolated from whole blood of healthy volunteers according to a protocol approved by the Institutional Review Board of Georgia Institute of Technology as previously described (35, 40). In brief, 5 ml of whole blood was collected using a sterile tube containing EDTA, then carefully layered over 3 ml of Histopaque (Sigma-Aldrich), centrifuged and washed 5 times with PBS and another 3 times with experimental additive solutions 45 (EAS45) at room temperature. The isolated RBCs were resuspended and stored in EAS45 solution at 10% hematocrit aseptically at 4°C for further protein coating and micropipette experiments.

Protein and antibodies

The following peptides were custom synthesized and purified: OVA-derived peptides OVA (SIINFEKL), E1 (EIINFEKL), K4 (SIIKFEKL), R4 (SIIRFEKL), and V-OVA (RGYNYEKL), vesicular stomatitis virus-derived peptide VSV (RGYVYQGL) (10, 37), lymphocytic choriomeningitis virus-derived peptide gp33 (KAVYNFATM) (38) and HIV-1 SF2 Gag protein-derived peptide HIV gag (SQVTNPANI) (41). Monomeric mouse MHC molecules complexed with these peptides (OVA, K4, R4, V-OVA, or VSV for H-2K^b and gp33 or HIV gag for H-2D^b) and tagged with a single biotin at the C terminus were produced by the National Institutes of Health Tetramer Core Facility at Emory University.

Rat anti-mouse CD8α (CT-CD8a) and CD8β (CT-CD8b) mAbs with or without PE conjugation were from Invitrogen. Rat anti-mouse Vα2 TCR (B20.1) mAb with or without PE conjugation was obtained from BD Pharmingen or eBioscience, respectively. PE-conjugated hamster anti-mouse CD3ε (145-2C11) mAb was purchased from BD Pharmingen. PE-conjugated anti-mouse H-2K^b (3H2672) and H-2D^b (BCDb) mAbs were obtained from U.S. Biological and Biocarta, respectively. PE-conjugated mouse anti-biotin (Bio3–18E7.2) mAb was purchased from Miltenyi Biotec.

Coupling pMHC onto RBCs

Biotin-streptavidin coupling was used to coat biotinylated pMHC monomers onto the RBC surface (40). RBCs were biotinylated using Biotin-X-NHS (Calbiochem) according to the manufacturer's instruction. In brief, RBCs were washed three times with PBS, incubated with titrated Biotin-X-NHS at pH 7.2 for 30 min at room temperature, and washed five times with PBS/1% BSA to remove Biotin-X-NHS and stop the reaction. The biotinylation efficiency was checked via flow cytometry by using PE-conjugated anti-biotin mAb. After three washes with EAS45/1% BSA, biotinylated RBCs were stored in EAS45 solution for further use within 3–4 wk.

Before each experiment, biotinylated RBCs were incubated with streptavidin (Pierce) at 0.5 mg/ml for 30 min at 4°C, washed three times with EAS45/1% BSA to remove unbound streptavidin, and incubated with biotinylated pMHC monomers for 30 min at 4°C. After washing three times with EAS45/1% BSA, the pMHC coated RBCs were ready for site density determination and micropipette adhesion assay.

Determination of molecular density on cell surface

For every micropipette experiment, site densities of pMHC on RBCs and CD8 on T cells were measured by flow cytometry (Fig. 1). To measure the pMHC site density, RBCs were incubated with PE-conjugated mAb 3H2672 (for H-2K^b) or BCDb (for H-2D^b) at 10 μg/ml in 200 μl of FACS buffer (RPMI 1640/5 mM EDTA/1% BSA/0.02% sodium azide) on ice for 40 min. Similarly, CD8α subunit, CD8β subunit, TCR, and CD3 expressed on T cells were stained with their respective PE-conjugated mAbs. CD8 is expressed as either an $\alpha\alpha$ homodimer or an $\alpha\beta$ heterodimer (1). Therefore, it is assumed that the site density of CD8$\alpha\beta$ equals that of CD8β whereas the site density of CD8$\alpha\alpha$ equals half of the site density difference between CD8α and CD8β.

Micropipette adhesion frequency assay

2D kinetics of MHC-CD8 interactions were measured using a micropipette adhesion frequency assay modified from that described previously (35). In brief, a pMHC-coated RBC and a T cell were aspirated by two apposing micropipettes with respective diameters of 1.5 and 3 μm in isotonic chamber medium (L-15/5 mM HEPES/1% BSA). Adhesion between the RBC and the T cell was staged by placing the cells into controlled contact via micromanipulation (Fig. 2). The presence of adhesion at the end of a given contact period was detected mechanically by observing microscopically the deflection of the soft RBC membrane upon retracting it away from the T cell. Such detection was reliable and unambiguous in >90% of the tests, as clearly observable membrane deflections could be generated by a force as low as 2 pN at the RBC apex. This approach-contact-retraction cycle was repeated 50 times to calculate an adhesion frequency, P_a, at that contact duration, t. For each pMHC, >30 pairs of cells were used to obtain several P_a vs t curves that correspond to different CD8 and pMHC densities, m_r and m_l. Each binding curve was fitted using nonlinear regression to the following probabilistic kinetic model for single-step monovalent receptor-ligand interaction (35),

$$P_a = 1 - \exp\{-m_r m_l A_c K_a^0 [1 - \exp(-k_r^0 t)]\}, \quad (1)$$

to estimate a pair of parameters: a zero-force reverse-rate, k_r^0, and an effective binding affinity, $A_c K_a^0$, where A_c is the contact area (which was kept constant in all experiments). Means and SEs of k_r^0 and $A_c K_a^0$ were calculated from their individual values estimated from different P_a vs t curves corresponding to different m_r and m_l for each pMHC.

Two variant forms of Equation 1 were used in data analysis. The first form is a log transformation of Equation 1 at $t \to \infty$,

$$\ln[1 - P_a(\infty)]^{-1} = A_c K_a^0 \cdot m_r m_l, \quad (2)$$

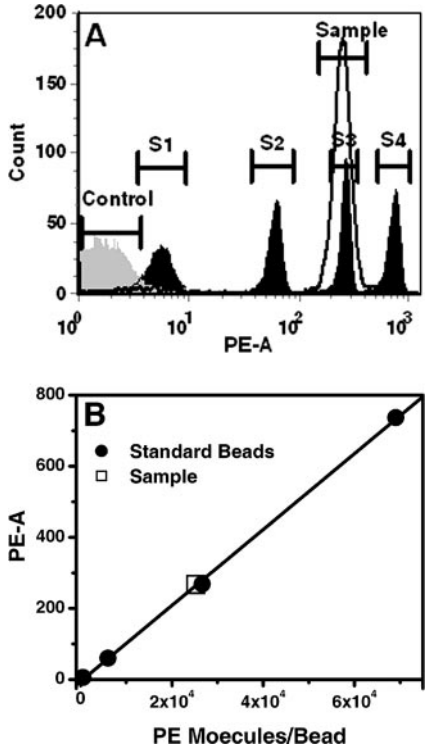

FIGURE 1. Site density determination. *A*, T cells were incubated with PE-labeled primary mAb and analyzed by flow cytometry (*sample, open histogram*) along with four standard calibration beads (*S1–S4*, *filled histograms*). The isotype control for nonspecific binding was shown for comparison (*control, shaded histogram*). *B*, A calibration curve of PE molecules/bead (provided by manufacturer) vs measured fluorescence intensity PE-A was plotted based on data of four standard beads (*filled circles*). The site density of CD8 on T cells was calculated by comparing the fluorescence intensity of the sample (*open square*) with the calibration curve after subtracting negative control fluorescence intensity.

which predicts that the transformed adhesion frequency, $\ln[1 - P_a(\infty)]^{-1}$, is proportional to the product of the CD8 and pMHC densities, $m_r m_l$, with the effective binding affinity, $A_c K_a^0$, as the constant of proportionality. The second form is to normalize the adhesion frequency by dividing the molecular site densities after the log transformation, but keep the time dependence:

$$\ln(1 - P_a)^{-1}/m_r m_l = A_c K_a^0[1 - \exp(-k_r^0 t)]. \quad (3)$$

Applying the log transformation and normalization according to Equation 3 is predicted to collapse a family of P_a vs t curves corresponding to different m_r and m_l into a single curve, provided that they correspond to the same set of kinetic reverse-rate and effective affinity.

Results

Isolation of MHC-CD8 binding from the trimolecular TCR-MHC-CD8 interaction

The micropipette adhesion frequency assay is illustrated in Fig. 2. A mouse T cell and a human RBC were respectively aspirated by two apposing micropipette (Fig. 2*A*). Cells were then brought into controlled contact (Fig. 2*B*), and subsequently moved apart to determine whether an adhesion was present (Fig. 2*C*) or not (Fig. 2*D*) at the end of the contact period.[4] To determine binding kinetics in this mechanical manner, the receptor-ligand bond involved has to be able to sustain a minimum force detectable by the RBC pico-force sensor (35). This is indeed the case for the MHC-CD8 interaction in question. An adhesion event between a T cell and RBC was unambiguously observed from the RBC membrane elongation, which resulted from the molecular force anchoring the RBC apex to the T cell (Fig. 2*C*). This was distinctly different from a nonadhesion event in which the RBC membrane readily separated from the T cell as the micropipette retracted (Fig. 2*D*). Although in any particular contact test both positive (i.e., adhesion) as well as negative (i.e., no adhesion) outcomes were possible and random, the probability of adhesion P_a was determined by the contact area A_c and time t, the densities of receptors m_r and ligands m_l, as well as the reverse-rate k_r^0 and binding affinity K_a^0, as predicted by Equation 1. Rather than adhesion force, the adhesion frequency assay measures this probability by counting adhesion frequency in repeated contact tests (35).

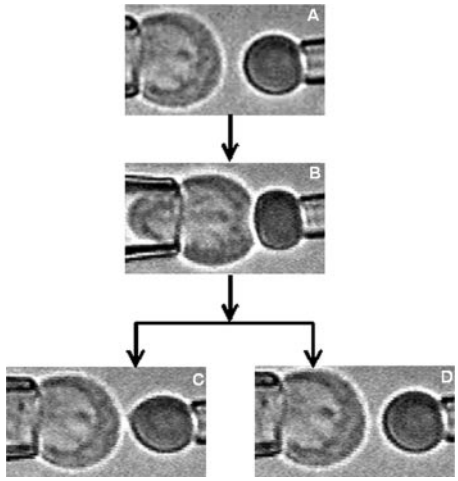

FIGURE 2. Micropipette adhesion frequency assay. A micropipette-aspirated T cell (*A*, *left*) was driven by a piezoelectric translator to make a controlled contact with a RBC coated with MHC held stationary by another pipette (*B*, *right*). At the end of the contact period, the computer-driven translator retracted the pipette to the starting position. An adhesion, if present, would result in elongation of the RBC upon its retraction, enabling visual detection of the adhesion (*C*). The RBC membrane would retract away from the T cell surface smoothly if there was no adhesion (*D*). (Also see Supplementary Video.)

CTLs express both TCR and CD8, which may bind different sites on the same or different pMHCs (12, 18, 37). A given TCR is capable of binding different peptides complexed with MHC of the same allele with different kinetic rates and affinities, which can differentially trigger T cell activation (10, 11). To isolate MHC-CD8 binding from trimolecular TCR-MHC-CD8 interactions, an anti-TCR Vα2 mAb (B20.1) was used to block TCR-MHC binding. Also, an anti-CD8α blocking mAb (CT-CD8a) was used to confirm that, apart from a low level background, the measured binding was predominately due to specific MHC-CD8 interaction. T cells expressing a monoclonal TCR from transgenic mice were preincubated with 50 μg/ml anti-TCR Vα2 or 10 μg/ml anti-CD8α for 30 min at 4°C and micropipette assays were performed in the continuous presence of the same concentrations of mAbs. In this study, TCR-independent, MHC-CD8 specific interactions were isolated for the three types of T cells (OTI, P14, and F5) used and for all pMHCs tested, including the peptides listed in Tables I and II bound to either H-2K^b or H-2D^b MHC alleles. Some of the results are exemplified in Fig. 3 using H-2K^b complexed with three peptides with various properties for OTI T cells—VSV (null), R4 (antagonist), and OVA (agonist) (10, 37).

For the null peptide VSV (Fig. 3*A*), micropipette adhesion tests in the absence of Ab yielded an adhesion frequency that increased with contact duration initially then reached a steady state (□). Addition of the anti-CD8α mAb completely abolished binding at

[4] The online version of this article contains supplemental material.

Table I. *Kinetic parameters for OTI TCR-independent, CD8-mediated binding to H-2K^b MHC*

H-2K^b pMHC	m_r (μm^{-2})	m_l (μm^{-2})	k_r^0 (s^{-1})	$A_cK_a^0$ (10^{-6} μm^4)
VSV	305	820	1.53 ± 0.37	2.32 ± 0.24
VSV	297	715	0.88 ± 0.48	5.72 ± 1.79
VSV	297	126	1.63 ± 1.01	8.06 ± 1.91
VSV	233	1661	1.58 ± 0.30	5.25 ± 0.55
VSV	326	1254	2.52 ± 0.61	5.53 ± 0.62
VSV	370	434	1.53 ± 0.24	5.10 ± 0.36
VSV	404	544	2.22 ± 0.24	7.20 ± 0.34
	Combined data		1.53 ± 0.22	5.75 ± 0.31
V-OVA	404	158	0.87 ± 0.18	7.74 ± 0.78
V-OVA	338	499	1.08 ± 0.34	6.90 ± 1.17
V-OVA	233	1529	2.00 ± 0.17	5.63 ± 0.48
	Combined data		1.12 ± 0.15	6.66 ± 0.36
OVA	281	1659	0.68 ± 0.14	3.58 ± 0.47
OVA	198	844	1.14 ± 0.25	3.33 ± 0.34
	Combined data		0.83 ± 0.12	3.51 ± 0.22
K4	290	648	1.04 ± 0.17	6.13 ± 0.52
R4	276	761	1.55 ± 0.15	3.25 ± 0.13

all contact durations tested (○), suggesting that the measured adhesion between T cells and RBCs was solely mediated by the specific MHC-CD8 interaction. This was further supported by the lack of effect of the anti-TCR Vα2 mAb which yielded a binding curve (△) indistinguishable from that without Ab (□). Similar results were obtained for another null peptide K4 (data not shown). The inability to detect TCR binding indicated that OTI TCR did not recognize the null peptides. This agreed with results from other assays including SPR measurement (10, 11), synapse formation, and fluorescence resonance energy transfer measurement (37). The results also indicated that anti-TCR Vα2 mAb did not sterically hinder MHC-CD8 interactions. Thus, binding of RBCs bearing MHC complexed with null peptides to T cells is measurable, TCR-independent, and MHC-CD8 specific. We also tested the effect of anti-TCR Vα2 mAb on binding between P14 T cells and RBCs coated with H-2K^b VSV pMHC and obtained similar results (data not shown). These data allowed us to use null pMHCs to measure the specific MHC-CD8 interaction in future experiments without using anti-TCR mAbs.

For antagonist peptide R4 (Fig. 3*B*), micropipette adhesion tests in the absence of Ab yielded much higher adhesion frequencies at all contact durations compared with VSV at equivalent site densities (□, compare Fig. 3, *A* and *B*). These adhesions, especially those at contact durations >2 s, were also stronger, as it was more difficult to separate the RBC from the T cell. When the anti-TCR Vα2 mAb was added, however, the adhesion frequency dropped to levels that matched those mediated by the binding of CD8 to VSV pMHC at corresponding contact durations (△, compare Fig. 3, *A* and *B*). Thus, there was a significant contribution from the TCR-MHC interaction to the measured adhesion when the antagonist R4 was used. This also ruled out the possibility that, when the peptide was VSV, the lack of blocking was due to problems with the anti-TCR Vα2 mAb (Fig. 3*A*). Addition of anti-TCR Vα2 and anti-CD8α mAbs to block both TCR and CD8 completely abrogated adhesion (◇), suggesting that binding in the presence of anti-TCR Vα2 alone (△) was mediated solely by specific MHC-CD8 interaction. Similar data were obtained for another antagonist V-OVA (data not shown). Thus, both TCR and CD8 bind MHC complexed with antagonist peptides R4 or V-OVA, and the specific MHC-CD8 interaction can be isolated by blocking the TCR-pMHC interaction using the anti-TCR Vα2 mAb.

Table II. *Kinetic parameters for OTI TCR-independent, CD8-mediated binding to H-2D^b MHC*

H-2D^b pMHC	m_r (μm^{-2})	m_l (μm^{-2})	k_r^0 (s^{-1})	$A_cK_a^0$ (10^{-7} μm^4)
gp33	233	1157	0.55 ± 0.17	7.81 ± 1.22
HIV gag	326	1713	0.55 ± 0.12	5.14 ± 0.60

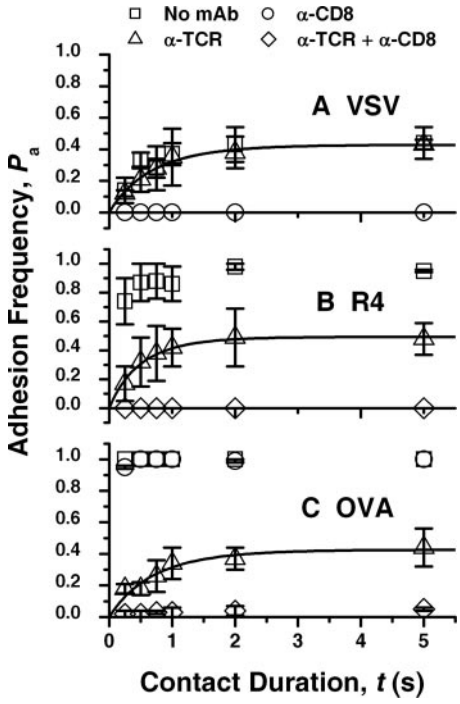

FIGURE 3. Isolation of MHC-CD8 binding from TCR-MHC-CD8 interaction. Plots of adhesion frequency vs contact duration measured using T cells from OTI TCR transgenic mice interacting with RBCs coated with H-2K^b MHC complexed with null peptide VSV (*A*), antagonist peptide R4 (*B*) and agonist peptide OVA (*C*) in the absence (□) or presence of blocking mAb(s) against TCR (Δ), CD8 (○), or both (◇). Data (*points*) were presented as mean ± SEM (or single value) of 1–5 pairs of T cells and RBCs each making 50 contacts to observe the frequency of adhesion. Using independently measured CD8 (m_r) and MHC (m_l) site densities, Equation 1 was fit (*curves*) to the anti-TCR Vα2 blocked data set (Δ) to estimate a pair of kinetic parameters, a reverse-rate k_r^0 and a 2D effective binding affinity $A_cK_a^0$.

For the agonist peptide OVA (Fig. 3*C*), micropipette adhesion tests in the absence of Ab yielded adhesion in every single test (i.e., 100% adhesion frequency) at all contact durations (□). These adhesions were even stronger than those mediated by R4 pMHC, as it was sometimes impossible to separate the RBC from the T cell, despite the fact that the pMHC densities on RBCs were matched for all three peptides (VSV, R4, and OVA). Also, addition of the anti-CD8α mAb alone did not lower the frequency of adhesions (○), although they appeared somewhat weaker. This indicates that OTI TCR interacted with agonist (OVA) pMHC much more strongly than antagonist (R4 or V-OVA) pMHC. When the anti-TCR Vα2 mAb was added, however, the adhesion frequency dropped to levels similar to those mediated by binding of CD8 to VSV-loaded MHC at corresponding contact durations (△, compare Fig. 3, *A* and *C*). Again, addition of mAbs to block both TCR and CD8 completely abrogated adhesion (◇), suggesting that binding in the presence of anti-TCR Vα2 alone (△) was mediated by specific MHC-CD8 interaction. Thus, both TCR and CD8 bind MHC complexed with agonist pMHC, and the specific MHC-CD8 interaction can be isolated by blocking the TCR-MHC interaction using the anti-TCR Vα2 mAb.

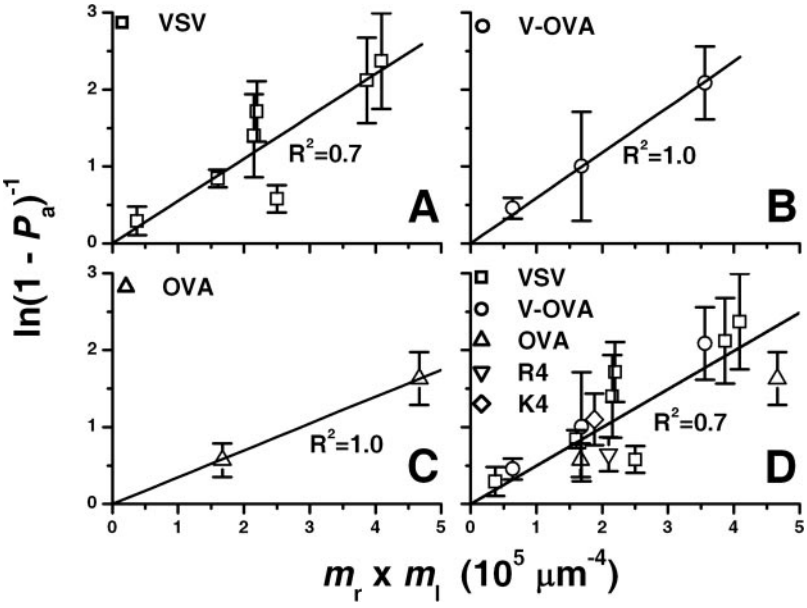

FIGURE 4. Effects of molecular site density on adhesion frequency. Adhesion frequency P_a was measured at 5 s contact duration from 2 to 7 pairs of T cells and RBCs (each making 50 contacts) per data point. P_a was transformed according to the left-hand side of Equation 2 by taking a natural log of the reciprocal of the frequency of no adhesion to yield $\ln(1 - P_a)^{-1}$, then plotted vs the product of the CD8 and MHC site densities, $m_r m_l$, for H-2K^b MHC complexed with VSV (*A*), V-OVA (*B*), and OVA (*C*) peptides separately. The data from panels *A–C* were pooled in panel *D* on which data from two other peptides, R4 and K4, were also plotted. The error bars were computed from SEM of P_a according to the Gaussian error propagation law. A straight line with zero *y*-intercept was fit to data in each panel. The goodness-of-fit was indicated by the R^2 values.

As an additional control, biotinylated RBCs not coated with pMHC were tested against T cells, which produced <2% adhesion regardless of the T cell specificity (data not shown). Thus, no adhesion molecules other than pMHC on RBCs and TCR and CD8 on T cells contribute to the adhesion frequencies measured with the micropipette adhesion assay.

To rule out the possibility that anti-TCR Vα2 mAb might cause changes in CD8 expression, we incubated OTI T cells with anti-TCR Vα2 mAb (50 μg/ml) in chamber medium (L-15/5 mM HEPES/1% BSA) for 90 min, which was the time elapse of a typical micropipette experiment, then stained with PE-conjugated anti-CD8 mAbs in FACS buffer to quantify the expressions of CD8α and CD8β by flow cytometry. We also stained T cells not preincubated with anti-TCR Vα2 mAb with the same anti-CD8α and anti-CD8β mAbs as a control. CD8 expression was indistinguishable (data not shown), indicating that anti-TCR Vα2 mAb did not alter CD8 expression. It must be stressed that to detect the low affinity specific MHC-CD8 interaction, we had to use very high MHC site densities ($\sim$1000 sites/μm^2). In sharp contrast, $\sim$10 sites/μm^2 of OVA pMHC were sufficient to produce a specific trimolecular TCR-MHC-CD8 binding comparable to the TCR-independent MHC-CD8 binding (data not shown).

Stoichiometry of the MHC-CD8 interaction

The density m_r of CD8 expressed on OTI T cells slightly varied from mouse to mouse. The density m_l of MHC coated on RBCs also varied depending on the coating conditions. How CD8 and MHC densities regulate the adhesion frequency P_a (through mass action) depends on the stoichiometry, or valency, of the MHC-CD8 interaction. To determine this valency, we took the natural log of the reciprocal of the probability of no adhesion, $\ln(1 - P_a)^{-1}$, measured at 5 s contact duration and plotted it against the product of the site densities, $m_r m_l$, for several pMHC ligands (Fig. 4). The data in Fig. 3 show that MHC-CD8 binding had achieved steady state at 5 s. Equation 2 predicts that the $\ln[1 - P_a(\infty)]^{-1}$ vs $m_r m_l$ plots should be linear with a zero *y*-intercept and a slope equal to the 2D effective binding affinity, $A_c K_a^0$, provided that CD8 binds pMHC monovalently. This prediction is supported by the data for CD8 on OTI T cells interacting with MHC complexed with the null peptide VSV coated on RBCs measured using seven $m_r m_l$ values (Fig. 4*A*). It is evident that the data points are evenly scattered around a straight line that passes through the origin. Equation 2 is also supported by data from MHC complexed with different peptides, e.g., antagonist peptide V-OVA (Fig. 4*B*) and agonist peptide OVA (Fig. 4*C*), obtained using anti-TCR Vα2 blocking. The data from Fig. 4, *A–C*, are pooled in Fig. 4*D* along with additional data measured using the same MHC allele (H-2K^b) complexed with two other peptides, antagonist peptide R4 and null peptide K4. These data indicate that T cell CD8 forms monomeric bonds with MHC despite the fact that MHC was decorated on the RBC surface via biotin-streptavidin coupling, which might form dimers.

Evaluation of kinetic parameters for MHC-CD8 interactions

Having confirmed the 1:1 stoichiometry of MHC-CD8 interaction, Equation 1 was fit to the TCR-independent, CD8-mediated binding data to evaluate the kinetic parameters, k_r^0 and $A_c K_a^0$, for various MHC-CD8 interactions studied in this work, as exemplified in Fig. 3. Table I summarizes the kinetic parameters so evaluated for OTI T cell CD8 interacting with H-2K^b MHC complexed with five peptides for each pair of CD8 and pMHC densities tested (indicated). It is evident that, for each peptide, the kinetic parameters evaluated from individually fitting different P_a vs *t* data sets agree well, despite the fact that they correspond to different m_r and m_l levels, as expected from the monovalency of the MHC-CD8 interaction, which also demonstrates reproducibility of our assay. To further test the reliability of these best-fit parameter values, the mean k_r^0 and $A_c K_a^0$ values were calculated and used, along with the corresponding m_r and m_l values measured from independent flow cytometry experiments, to predict each P_a vs *t* data set, which shows excellent agreement, as exemplified in Fig. 5*A* for V-OVA.

MHC-CD8 interaction is peptide independent

Although differing in amino acid sequences and molecular weights, the five peptides listed in Table I were complexed with MHC of the same allele, H-2K^b. Cocrystal structures of pMHC:CD8 complexes show no contact between CD8 and the peptide (18). However, it is still possible that a peptide could influence MHC-CD8 interaction should its binding induce a conformational change in the MHC that would alter the CD8 binding site. In Fig. 4*D*, the $\ln[1 - P_a(\infty)]^{-1}$ vs $m_r m_l$ data from all five peptides appear to line up, suggesting that their binding affinities (equal to

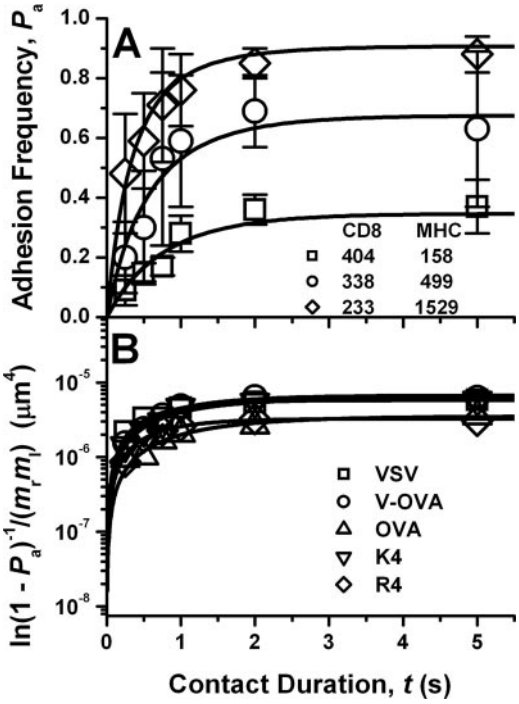

FIGURE 5. MHC-CD8 interaction is monovalent and peptide independent. *A*, Adhesion frequency was plotted against contact duration for each set of CD8 and V-OVA pMHC densities. Data (*points*) from three sets of site densities (indicated), each obtained from 15 to 29 pairs of OTI T cells and RBCs contacting 50 times each, were presented as mean ± SEM at each contact duration. Equation 1 was fit to each data set to evaluate a pair of kinetic parameters, k_r^0 and $A_cK_a^0$, the values of which are summarized in Table I along with the site densities. The mean values of k_r^0 and $A_cK_a^0$ (see Table I) were then used to predict theoretical binding curves for all three set of site densities (*curves*). The excellent agreement between experiment and theory supported the assumption on which Equation 1 was based, that the MHC-CD8 interaction is monovalent. *B*, Mean adhesion frequency data were transformed according to the left-hand side of Equation 3 and plotted vs the contact duration (*points*). The right-hand side of Equation 3 predicts that binding curves so plotted would depend only on the k_r^0 and $A_cK_a^0$ values of the interactions involved.

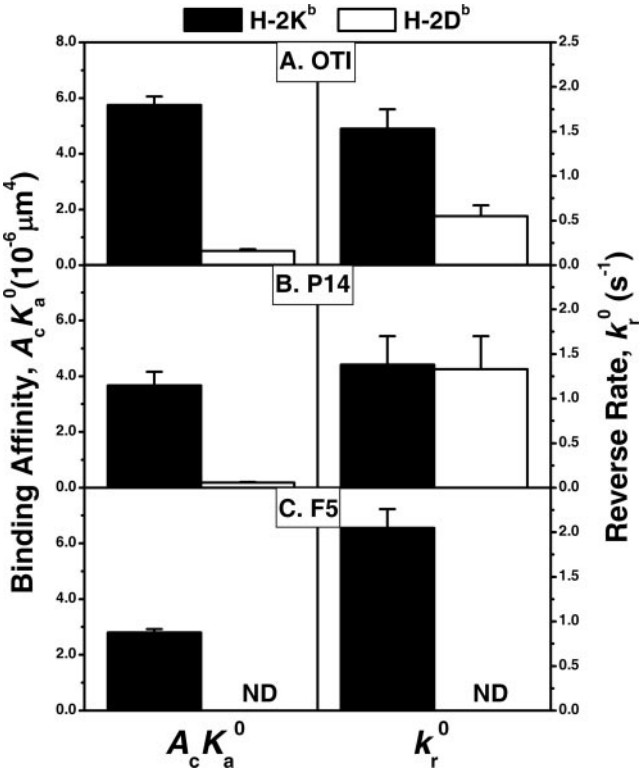

FIGURE 6. Dependence of MHC-CD8 binding on MHC alleles and T cell types. 2D effective binding affinity (*left column*) and kinetic reverse-rate (*right column*) of naive CTLs from three transgenic mice, OTI (*A*), P14 (*B*), and F5 (*C*), interacting with either H-2K^b (*solid bars*) or H-2D^b (*open bars*) were compared. Data were presented as mean ± SEM. ND = not detectable.

the slope of the line) have similar values. In Fig. 3, the TCR-independent, CD8-mediated P_a vs t data (Δ) appear to have similar shapes and plateau levels regardless of the peptide used, indicating similar kinetic parameters. It can be seen from the binding affinities and reverse-rates listed in Table I that these are indeed comparable for all five H-2K^b pMHCs.

To visualize the peptide independence of the kinetic parameters for the TCR-independent, CD8-mediated binding to MHC, we make use of Equation 3, which predicts that the $\ln(1 - P_a)^{-1}/m_r m_r$ vs t data depend only on the kinetic parameters. Data for MHC complexed with all five different peptides were plotted in Fig. 5*B* (points). The collapse of data demonstrates graphically that these interactions have comparable kinetic parameters. Conversely, similar kinetic parameters predict similar $\ln(1 - P_a)^{-1}/m_r m_r$ vs t curves, as shown by using the mean best-fit k_r^0 and $A_cK_a^0$ values for each peptide to plot the right-hand side of Equation 3 (Fig. 5*B*, curves), which overlay regardless of the peptide as predicted.

To further test our hypothesis that the MHC-CD8 interaction is peptide independent, kinetic parameters were measured for OTI T cells interacting with RBCs coated with H-2D^b MHC complexed with gp33 or HIV gag, which are null peptides not recognized by OTI TCR. As can be seen from Table II where data are listed, the corresponding $A_cK_a^0$ and k_r^0 values are very similar for the two peptides tested. Taken together, the data suggest that loading different peptides on MHC does not induce enough change in the CD8 binding site to affect the measured kinetic parameters of the MHC-CD8 interactions. In other words, the interactions between CD8 and pMHC are peptide-independent.

CD8 binds different MHC alleles with distinct kinetics

Using MHC tetramer staining and SPR experiment with purified molecules, Moody et al. found that CD8 bound H-2K^b MHC with higher avidity/affinity than H-2D^b MHC (25). Our 2D kinetic data support this finding. As shown in Fig. 6, CD8 from OTI T cells and P14 T cells respectively bound H-2K^b MHC with 7- and 20-fold higher 2D effective binding affinities than H-2D^b MHC, respectively (Fig. 6, *A* and *B*, *left column*). We were unable to measure kinetic parameters for F5 T cell CD8 interacting with H-2D^b MHC despite multiple attempts, because the affinity is too low to yield appreciable adhesion frequencies even at the highest MHC coating density we could achieve, which could measure affinity as low as $\sim 10^{-8}$ μm^4. However, the interaction between F5 T cell CD8 and H-2K^b MHC was readily measurable, resulting in a 2D effective binding affinity of $A_cK_a^0 = 2.8 \times 10^{-6}$ μm^4 (Fig. 6*C*, *left column*). Thus, the affinity of F5 T cell CD8 for H-2K^b MHC was two orders of magnitude higher than that for H-2D^b MHC. The impact of MHC allele on the reverse-rate of CD8 dissociation is less clear. CD8 from OTI T cells dissociated 3-fold more rapidly from H-2K^b than H-2D^b MHC (Fig. 6*A*, *right column*). By comparison CD8 from P14 T cells dissociated from H-2K^b and H-2D^b MHC with similar reverse-rates (Fig. 6*B*, *right column*).

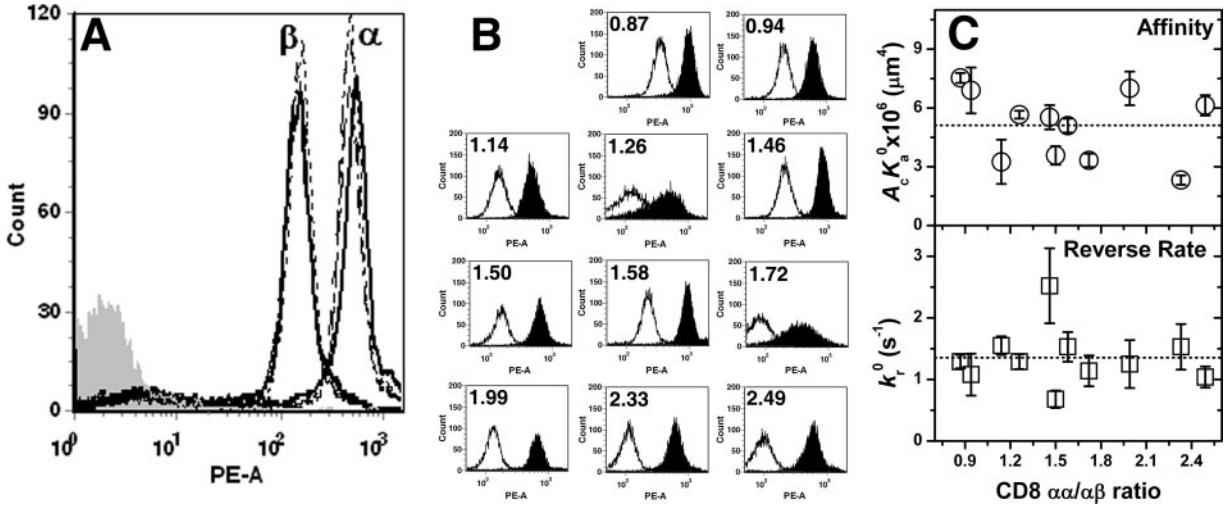

FIGURE 7. Lack of effect on CD8$\alpha\alpha$ and CD8$\alpha\beta$ expression. *A*, CD8α (α) and CD8β (β) expression levels on T cell were compared before interaction (*open histogram*) or after interaction with OVA (*dash histogram*), R4 (*dot histogram*) or VSV (*dash-dot histogram*) pMHC coated RBCs in the presence of anti-Vα2 mAb (50 μg/ml). Isotype control for nonspecific binding is shown as shaded histogram. Part of some histograms are obscured due to overlapping. *B*, Flow cytometric analysis for the expression of CD8α (*filled histograms*) and CD8β (*open histograms*) on 11 batches of OTI T cells. The ratio value of CD8$\alpha\alpha$/CD8$\alpha\beta$ was indicated on each small panel. *C*, 2D effective binding affinity ($A_cK_a^0$, *upper panel*) and kinetic reverse-rate (k_r^0, *lower panel*) measured using these 11 batches of OTI T cells were plotted against the CD8$\alpha\alpha$/CD8$\alpha\beta$ ratio and compared with the average affinity or average reverse rate (*dash lines*). Data were presented as mean ± SEM.

The same MHC allele binds CD8 from different T cells with different affinities

Unexpectedly, CD8 on T cells from different TCR transgenic mice was found to bind the same allelic pMHC with different affinities; the H-2K^b MHC binding affinity for CD8 on OTI T cells was 50% and 100% more than those on P14 T cells and from F5 T cells, respectively (compare the three panels in Fig. 6, solid bars, *left column*). A similar trend was found for the H-2D^b MHC, which bound OTI T cell CD8 with an affinity 2- (compare *A* and *B* in Fig. 6, open bars, *left column*) and >10-fold more than those of P14 and F5 T cell CD8, respectively. To exclude the possibility that CD8 expression was changed by repeated touches with a pMHC coated RBC during the micropipette assay, OTI T cells were first incubated with 50 μg/ml anti-TCR Vα2 mAb for 30 min, mixed with OVA, R4 or VSV pMHC coated RBCs at a ratio of 1:100 in the presence of anti-TCR Vα2 mAb, pelleted the cells and incubated at room temperature for 10 min. After the RBCs were lysed with lysis buffer (eBioscience), the T cells were stained with anti-CD8α or β mAb to compare the CD8 expression levels. Flow cytometry data showed the CD8 expression level did not alter (Fig. 7*A*).

CD8$\alpha\beta$ is believed to be a more potent coreceptor than CD8$\alpha\alpha$. Therefore, we hypothesized that CD8$\alpha\beta$ bound MHC better than CD8$\alpha\alpha$, and that CD8 expressed on OTI, P14, and F5 T cells with different CD8$\alpha\alpha$/CD8$\alpha\beta$ ratios. However, flow cytometry results showed that the CD8$\alpha\alpha$/CD8$\alpha\beta$ ratios were comparable for those three types of T cells (data not shown). To further test this hypothesis, we took advantage of the fact that the site densities of CD8$\alpha\alpha$ and CD8$\alpha\beta$ varied mildly among OTI T cells purified from different transgenic mice, with site density ratios of CD8$\alpha\alpha$/CD8$\alpha\beta$ ranging from 0.9–2.5 (indicated in the upper-left corner of each panel in Fig. 7*B*). In the preceding section, we have shown that the MHC-CD8 binding affinity and reverse-rate are independent of the peptide. Here we plot the 2D effective binding affinity

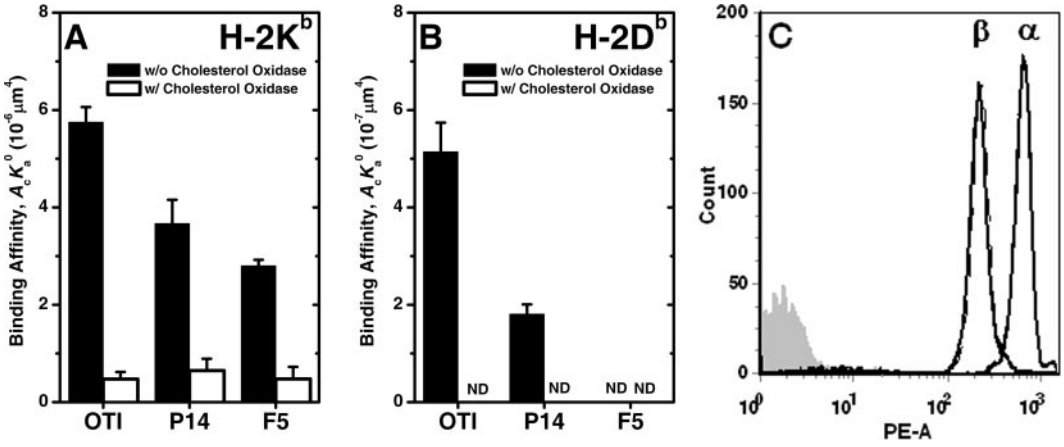

FIGURE 8. Reduction of MHC-CD8 affinity by cholesterol oxidase treatment. *A* and *B*, 2D binding affinities of H-2K^b (*A*) or H-2D^b (*B*) MHC for CD8 on three T cells with (*open bars*) or without (*solid bars*) cholesterol oxidase treatment. Data were presented as mean ± SEM. ND = not detectable. *C*, The CD8α and CD8β expression levels of F5 T cells treated with 1 U/ml cholesterol oxidase (*dash histogram*) were compared with untreated T cells (*open histogram*, which overlaps with the *dash histogram*). Isotype control for nonspecific binding is shown as shaded histogram.

Table III. *Binding affinities of MHC-CD8 with (+) or without (−) cholesterol oxidase treatment*

T Cell	H-2K^b (−)	H-2K^b (+)	H-2D^b (−)	H-2D^b (+)
OTI (10^{-6} μm^4)	5.75 ± 0.31	0.47 ± 0.15	0.51 ± 0.06	ND[a]
P14 (10^{-6} μm^4)	3.67 ± 0.49	0.65 ± 0.24	0.18 ± 0.02	ND[a]
F5 (10^{-6} μm^4)	2.80 ± 0.12	0.48 ± 0.25	ND[a]	ND[a]

[a] Not detectable.

(Fig. 7*C*, *upper panel*) or reverse-rates (Fig. 7*C*, *lower panel*) measured using eleven batches of OTI T cells vs the CD8$\alpha\alpha$/CD8$\alpha\beta$ ratio. It is evident that the two kinetic parameters $A_cK_a^0$ and k_r^0 measured from different batches of T cells scatter evenly around a horizontal line equal to their respective average values (dotted line in each panel of Fig. 7*C*), suggesting a lack of dependence on the CD8$\alpha\alpha$/CD8$\alpha\beta$ ratio. These data indicate that the difference in coreceptor potencies between CD8$\alpha\alpha$ and CD8$\alpha\beta$ in activating T cells does not manifest as difference in their binding kinetics for MHC.

Disruption of membrane rafts differentially reduces affinity for MHC of CD8 from different T cells and abolishes the affinity differences

The micropipette frequency assay measured interactions between molecules anchored on the apposing membranes of a RBC and a T cell. These interactions can be impacted by the cell surface environment, as previously shown for membrane microtopology and stiffness (33, 34). Another aspect of the membrane environment may be membrane rafts into which CD8 can partition (4). Membrane rafts, and/or the CD8 partitioning therein, could vary among the three transgenic T cells used in our study, thus altering the apparent MHC-CD8 affinity. To test this hypothesis, we measured 2D binding affinities after disrupting membrane rafts by incubating T cells with 1 U/ml cholesterol oxidase (MP Biomedicals) for 30 min (42, 43). Disruption of membrane rafts substantially reduced the MHC binding affinities for CD8 on all three T cells for both H-2K^b (Fig. 8*A*, compare the solid and open bars in each group, and Table III) and H-2D^b (Fig. 8*B*, adhesion became undetectable after cholesterol oxidase treatment despite that we used highest possible MHC site density, and Table III) alleles. This was not due to a decrease in the CD8 expression by the cholesterol oxidase treatment, as flow cytometry measurement using OTI or F5 T cells with and without such treatment showed identical CD8 expression levels (Fig. 8*C*). Also, treating RBCs with cholesterol oxidase alone did not affect MHC-CD8 binding (data not shown). Remarkably, cholesterol oxidase treatment reduced the H-2K^b MHC-CD8 binding affinity by different amounts in different T cells: 12-, 5.6-, and 5.8-fold in OTI, P14, and F5 cells, respectively. Thus, the H-2K^b MHC binding affinities for CD8 on different T cells were similar after rafts disruption (Fig. 8*A*, compare the three open bars and Table III). These results suggested that partitioning of CD8 in membrane rafts differentially enhanced its MHC binding affinity in the three T cells tested. The enhancement was abolished after the membrane rafts were disrupted, resulting in comparable CD8-MHC binding affinities regardless of the T cell specificity.

Discussion

The present work represents a first step toward dissecting the 2D molecular interactions between T cells and APCs, which involve a number of molecular players, including TCR, coreceptors, adhesion molecules, and costimulatory molecules. Some molecules provide physical linkages to bridge the two cell membranes and form junctional structures, while others deliver signals upon Ag recognition. Some interactions take place between binding partners respectively residing on apposing membranes of the T cell and the APC, while others occur between molecules both residing on the same membrane. Kinetic rates and binding affinity are important determinants for these molecular interactions, for such parameters are believed to correlate with T cell activation. Most published work used SPR for kinetic measurement, which uses purified molecules that have been isolated from their native T cell surface environment (3, 4, 10, 11, 23–25, 44, 45). Some studies use MHC tetramer or MHC-Ig dimeric molecules to stain T cells (6, 7, 16, 25, 46–50), but still measure 3D kinetic parameters. A few experiments measured 2D binding by a simple cell adhesion assay (21, 37, 51). However, this assay lacks sufficient temporal resolution to measure the kinetics of MHC-CD8 interactions. A different method has been used to measure 2D affinity, which visualizes bond formation between a receptor-expressing cell and a glass-supported lipid bilayer reconstituted with fluorescently labeled, lipid-anchored, freely mobile ligands (52–54). At physiological receptor and ligand densities, thousands of bonds are typically formed in a time scale of ~10 min, which is a large enough number of bonds and sufficiently long time to smoothen the self-assembled contact area. By comparison, the micropipette method detects binding in seconds on a rough T cell surface full of microvilli. These differences probably underlie the orders of magnitude of differences in the 2D affinities measured by the supported bilayer method and the micropipette method (31). Moreover, it required extension for this method to be used for measuring 2D kinetics (TP Tolentino, J Wu, VI Zarnitsyna, F Ying, ML Dustin, and C Zhu, unpublished data). Our paper reports the first 2D kinetic measurements using T cell CD8 to interact with pMHC presented on the membrane of RBCs. The measured effective binding affinities of TCR-independent MHC-CD8 interactions are much lower than those of selectin-ligand interactions (32, 55) and the high affinity integrin-ligand interactions (56) but are similar to the IgG binding affinities of the low affinity FcγRs CD16b (57) and CD32a (58).

There are two known receptors on the surface of CTLs for MHC: TCR and CD8. Multiple lines of evidence suggest that CD8 facilitates or enhances TCR to recognize Ag and initiate T cell activation, and it was shown that after abolishing the CD8 binding by making a mutation on the α3 domain of MHC, not only the tetramer staining efficiency for T cell was reduced, but the T cell activation was dramatically diminished (48). However, the detail mechanisms of cooperation between CD8 and TCR are not yet clear (1). One hypothesis proposes that binding of one molecule (CD8 or TCR) holds MHC to an optimal configuration, thereby accelerating the association of the other molecule (TCR or CD8) to MHC (5, 14). An alternative but related hypothesis proposes that binding of the second molecule (CD8 or TCR) to MHC stabilizes the interaction between the first molecule (TCR or CD8) and MHC, thereby decelerating the dissociation of both molecules from MHC (6, 24). These hypotheses imply cooperation between

TCR and CD8 at the level of MHC binding. Although SPR experiments did not find significant difference in the binding of solution MHC to immobilized TCR in the presence or absence of solution CD4/8 (3, 44), these negative data cannot rule out the possibility of cooperation when both TCR and CD8 reside on the same T cell membrane. The data in Fig. 3 show that inhibiting the TCR-MHC interaction by a blocking mAb does not result in detectable change in the kinetics of MHC binding to CD8 at a resting state. In other words, TCR-MHC and MHC-CD8 interactions appear to be independent at the level of adhesion measured by the present assay and the adhesion levels mediated by these two interactions are additive rather than synergistic, which provides a partial answer to the question of cooperation.

Cocrystal structures of both human and mouse pMHC:CD8 complexes reveal that CD8 mainly binds to the invariant $\alpha 3$ domain of the H chain and to the $\beta 2$-microglobulin subunit of MHC (12, 18). By comparison, cocrystal structures of TCR:pMHC complexes reveal that TCR interacts with the $\alpha 1$ and $\alpha 2$ domains of the H chain of MHC where the peptide cleft is located (2, 59). Thus, TCR and CD8 bind to spatially separated sites on MHC. Crystallographic studies also reveal little structural differences in MHC complexed with different peptides (2, 59). It is therefore not surprising to find that the kinetic parameters of the TCR-independent, CD8-mediated MHC binding are peptide independent (Figs. 3, 4*D*, and 5*B*, Tables I and II). Indeed, this conclusion has been supported by previous studies using SPR measurement (24) and the cell adhesion assay (37). Thus, unlike the TCR-MHC interaction, MHC-CD8 interaction is independent on the peptide potency in triggering T cell activation.

By comparison, different MHC alleles, such as H-2K^b and H-2D^b, may have sufficient structural differences to impact their CD8 binding kinetics (25, 45). In support of this hypothesis, we found that CD8 bound H-2K^b with a much higher affinity than H-2D^b for the three types of T cells tested (Fig. 6). This is consistent with previous SPR measurements, which found that binding of CD8 to H-2K^b MHC was at least 2-fold better than H-2D^b (25). Similar results were obtained for HLA-CD8 interactions in a human system, where CD8$\alpha\alpha$ bound differently to different alleles of HLA with subtle conformational differences in the $\alpha 3$ domain (45). The agreement of the present results with previous observations obtained using MHC tetramers, CD8 transfectants, and SPR supports the validity of the micropipette assay as applied to the T cells.

Cocrystal structures of human CD8$\alpha\alpha$:HLA-A2 (12) and mouse CD8$\alpha\alpha$:H-2K^b (18) complexes show that CD8$\alpha\alpha$ primarily binds the $\alpha 3$ domain of MHC asymmetrically in an Ab-like fashion. The first α subunit interacts with MHC $\alpha 3$ and $\beta 2$-microglobulin domains, which comprises of >70% of the contact surface. The second α subunit engages less and interacts only with the MHC $\alpha 3$ domain (12, 18). Although no crystal structure of MHC:CD8$\alpha\beta$ complex has been published yet, such structure has been modeled by replacing either CD8α subunit of CD8$\alpha\alpha$ with a CD8β subunit (17). Based on the model, Chang et al. proposed that, although CD8$\alpha\beta$ could bind MHC with two distinct orientations, the primary binding site was still the $\alpha 3$ domain of MHC and the basic interaction mode was the same as that of CD8$\alpha\alpha$ (17). By comparison, Devine et al. suggested that only the CD8α subunit could make a major contact with MHC class I (60). Nevertheless, both CD8$\alpha\alpha$ and CD8$\alpha\beta$ interact with MHC and promote TCR-MHC recognition (2), yet CD8$\alpha\beta$ is two orders of magnitude more efficient as a coreceptor than CD8$\alpha\alpha$ (20). However, it is controversial as to whether the different coreceptor efficiencies correspond to different MHC-CD8 binding. Sun et al. found that CD8$\alpha\alpha$ and CD8$\alpha\beta$ mediated similar levels of cell-cell adhesion (21). Similarly, SPR measurement found that CD8$\alpha\alpha$ and CD8$\alpha\beta$ had similar 3D affinities for H-2K^b MHC (22, 23, 25). By comparison, MHC tetramer staining experiment found that CD8$\alpha\beta$ mediated greater interactions with MHC than CD8$\alpha\alpha$, although this discrepancy might come from either the CD8 expressing transgenic mice or the H-2D^k MHC used (16). Our data suggest that the different coreceptor functions of CD8$\alpha\alpha$ and CD8$\alpha\beta$ are not due to their different 2D binding for MHC as they bind the same MHC allele with comparable 2D affinities and off-rates (Fig. 7).

Surprisingly, we found that CD8 expressed on different T cells bound the same MHC allele with different affinities (Fig. 6), and cholesterol oxidase treatment differentially reduced these affinities in different T cells. Remarkably, the 2D MHC-CD8 binding affinities became comparable for cholesterol oxidase treated T cells. These data are consistent with the hypothesis that partitioning of CD8 into membrane rafts differentially enhances its 2D binding affinity for MHC depending on the rafts in a particular type of T cells. Further studies are required to fully test this hypothesis and understand its implications to the regulation of MHC-CD8 interaction.

Acknowledgments

We thank N. Jiang, Y. Zhang, N. Pajic, C. Beal, S. Sambhara, and J. Plowden for technical assistance, N. Jiang for carefully reading the manuscript, and the National Institutes of Health Tetramer Core Facility at Emory University for providing MHC monomers.

Disclosures

The authors have no financial conflict of interest.

References

1. Cole, D. K., and G. F. Gao. 2004. CD8: adhesion molecule, co-receptor and immuno-modulator. *Cell. Mol. Immunol.* 1: 81–88.
2. Rudolph, M. G., R. L. Stanfield, and I. A. Wilson. 2006. How TCRs bind MHCs, peptides, and coreceptors. *Annu. Rev. Immunol.* 24: 419–466.
3. Wyer, J. R., B. E. Willcox, G. F. Gao, U. C. Gerth, S. J. Davis, J. I. Bell, P. A. van der Merwe, and B. K. Jakobsen. 1999. T cell receptor and coreceptor CD8 alphaα bind peptide-MHC independently and with distinct kinetics. *Immunity* 10: 219–225.
4. Arcaro, A., C. Gregoire, T. R. Bakker, L. Baldi, M. Jordan, L. Goffin, N. Boucheron, F. Wurm, P. A. van der Merwe, B. Malissen, and I. F. Luescher. 2001. CD8β endows CD8 with efficient coreceptor function by coupling T cell receptor/CD3 to raft-associated CD8/p56^{lck} complexes. *J. Exp. Med.* 194: 1485–1495.
5. Gakamsky, D. M., I. F. Luescher, A. Pramanik, R. B. Kopito, F. Lemonnier, H. Vogel, R. Rigler, and I. Pecht. 2005. CD8 kinetically promotes ligand binding to the T-cell antigen receptor. *Biophys. J.* 89: 2121–2133.
6. Campanelli, R., B. Palermo, S. Garbelli, S. Mantovani, P. Lucchi, A. Necker, E. Lantelme, and C. Giachino. 2002. Human CD8 co-receptor is strictly involved in MHC-peptide tetramer-TCR binding and T cell activation. *Int. Immunol.* 14: 39–44.
7. Daniels, M. A., and S. C. Jameson. 2000. Critical role for CD8 in T cell receptor binding and activation by peptide/major histocompatibility complex multimers. *J. Exp. Med.* 191: 335–346.
8. Delon, J., C. Gregoire, B. Malissen, S. Darche, F. Lemaitre, P. Kourilsky, J. P. Abastado, and A. Trautmann. 1998. CD8 expression allows T cell signaling by monomeric peptide-MHC complexes. *Immunity* 9: 467–473.
9. Lyons, G. E., T. Moore, N. Brasic, M. Li, J. J. Roszkowski, and M. I. Nishimura. 2006. Influence of human CD8 on antigen recognition by T-cell receptor-transduced cells. *Cancer Res.* 66: 11455–11461.
10. Alam, S. M., P. J. Travers, J. L. Wung, W. Nasholds, S. Redpath, S. C. Jameson, and N. R. Gascoigne. 1996. T-cell-receptor affinity and thymocyte positive selection. *Nature.* 381: 616–620.
11. Kersh, G. J., E. N. Kersh, D. H. Fremont, and P. M. Allen. 1998. High- and low-potency ligands with similar affinities for the TCR: the importance of kinetics in TCR signaling. *Immunity* 9: 817–826.
12. Gao, G. F., J. Tormo, U. C. Gerth, J. R. Wyer, A. J. McMichael, D. I. Stuart, J. I. Bell, E. Y. Jones, and B. K. Jakobsen. 1997. Crystal structure of the complex between human CD8$\alpha(\alpha)$ and HLA-A2. *Nature* 387: 630–634.
13. Gao, G. F., Z. Rao, and J. I. Bell. 2002. Molecular coordination of alphaβ T-cell receptors and coreceptors CD8 and CD4 in their recognition of peptide-MHC ligands. *Trends Immunol.* 23: 408–413.
14. Pecht, I., and D. M. Gakamsky. 2005. Spatial coordination of CD8 and TCR molecules controls antigen recognition by CD8+ T-cells. *FEBS Lett.* 579: 3336–3341.
15. Yachi, P. P., J. Ampudia, N. R. Gascoigne, and T. Zal. 2005. Nonstimulatory peptides contribute to antigen-induced CD8-T cell receptor interaction at the immunological synapse. *Nat. Immunol.* 6: 785–792.

16. Bosselut, R., S. Kubo, T. Guinter, J. L. Kopacz, J. D. Altman, L. Feigenbaum, and A. Singer. 2000. Role of CD8β domains in CD8 coreceptor function: importance for MHC I binding, signaling, and positive selection of CD8+ T cells in the thymus. *Immunity* 12: 409–418.
17. Chang, H. C., K. Tan, and Y. M. Hsu. 2006. CD8alphaβ has two distinct binding modes of interaction with peptide-major histocompatibility complex class I. *J. Biol. Chem.* 281: 28090–28096.
18. Kern, P. S., M. K. Teng, A. Smolyar, J. H. Liu, J. Liu, R. E. Hussey, R. Spoerl, H. C. Chang, E. L. Reinherz, and J. H. Wang. 1998. Structural basis of CD8 coreceptor function revealed by crystallographic analysis of a murine CD8alphaα ectodomain fragment in complex with H-2Kb. *Immunity* 9: 519–530.
19. Gangadharan, D., and H. Cheroutre. 2004. The CD8 isoform CD8alphaα is not a functional homologue of the TCR co-receptor CD8alphaβ. *Curr. Opin. Immunol.* 16: 264–270.
20. Devine, L., D. Thakral, S. Nag, J. Dobbins, M. E. Hodsdon, and P. B. Kavathas. 2006. Mapping the binding site on CD8 β for MHC class I reveals mutants with enhanced binding. *J. Immunol.* 177: 3930–3938.
21. Sun, J., and P. B. Kavathas. 1997. Comparison of the roles of CD8 α α and CD8 α β in interaction with MHC class I. *J. Immunol.* 159: 6077–6082.
22. Leishman, A. J., O. V. Naidenko, A. Attinger, F. Koning, C. J. Lena, Y. Xiong, H. C. Chang, E. Reinherz, M. Kronenberg, and H. Cheroutre. 2001. T cell responses modulated through interaction between CD8alphaα and the nonclassical MHC class I molecule, TL. *Science* 294: 1936–1939.
23. Kern, P., R. E. Hussey, R. Spoerl, E. L. Reinherz, and H. C. Chang. 1999. Expression, purification, and functional analysis of murine ectodomain fragments of CD8alphaα and CD8alphaβ dimers. *J. Biol. Chem.* 274: 27237–27243.
24. Garcia, K. C., C. A. Scott, A. Brunmark, F. R. Carbone, P. A. Peterson, I. A. Wilson, and L. Teyton. 1996. CD8 enhances formation of stable T-cell receptor/MHC class I molecule complexes. *Nature* 384: 577–581.
25. Moody, A. M., Y. Xiong, H. C. Chang, and E. L. Reinherz. 2001. The CD8alphaβ co-receptor on double-positive thymocytes binds with differing affinities to the products of distinct class I MHC loci. *Eur. J. Immunol.* 31: 2791–2799.
26. Viret, C., and C. A. Janeway, Jr. 1999. MHC and T cell development. *Rev. Immunogenet.* 1: 91–104.
27. Lee, N. A., D. Y. Loh, and E. Lacy. 1992. CD8 surface levels alter the fate of α/β T cell receptor-expressing thymocytes in transgenic mice. *J. Exp. Med.* 175: 1013–1025.
28. Robey, E. A., F. Ramsdell, D. Kioussis, W. Sha, D. Loh, R. Axel, and B. J. Fowlkes. 1992. The level of CD8 expression can determine the outcome of thymic selection. *Cell* 69: 1089–1096.
29. Call, M. E., and K. W. Wucherpfennig. 2005. The T cell receptor: critical role of the membrane environment in receptor assembly and function. *Annu. Rev. Immunol.* 23: 101–125.
30. Call, M. E., J. Pyrdol, M. Wiedmann, and K. W. Wucherpfennig. 2002. The organizing principle in the formation of the T cell receptor-CD3 complex. *Cell* 111: 967–979.
31. Dustin, M. L., S. K. Bromley, M. M. Davis, and C. Zhu. 2001. Identification of self through two-dimensional chemistry and synapses. *Annu. Rev. Cell Dev. Biol.* 17: 133–157.
32. Huang, J., J. Chen, S. E. Chesla, T. Yago, P. Mehta, R. P. McEver, C. Zhu, and M. Long. 2004. Quantifying the effects of molecular orientation and length on two-dimensional receptor-ligand binding kinetics. *J. Biol. Chem.* 279: 44915–44923.
33. Wu, L., B. Xiao, X. Jia, Y. Zhang, S. Lu, J. Chen, and M. Long. 2007. Impact of carrier stiffness and microtopology on two-dimensional kinetics of P-selectin and P-selectin glycoprotein ligand-1 (PSGL-1) interactions. *J. Biol. Chem.* 282: 9846–9854.
34. Williams, T. E., S. Nagarajan, P. Selvaraj, and C. Zhu. 2001. Quantifying the impact of membrane microtopology on effective two-dimensional affinity. *J. Biol. Chem.* 276: 13283–13288.
35. Chesla, S. E., P. Selvaraj, and C. Zhu. 1998. Measuring two-dimensional receptor-ligand binding kinetics by micropipette. *Biophys. J.* 75: 1553–1572.
36. Hogquist, K. A., S. C. Jameson, W. R. Heath, J. L. Howard, M. J. Bevan, and F. R. Carbone. 1994. T cell receptor antagonist peptides induce positive selection. *Cell* 76: 17–27.
37. Yachi, P. P., J. Ampudia, T. Zal, and N. R. Gascoigne. 2006. Altered peptide ligands induce delayed CD8-T cell receptor interaction–a role for CD8 in distinguishing antigen quality. *Immunity* 25: 203–211.
38. Kerry, S. E., J. Buslepp, L. A. Cramer, R. Maile, L. L. Hensley, A. I. Nielsen, P. Kavathas, B. J. Vilen, E. J. Collins, and J. A. Frelinger. 2003. Interplay between TCR affinity and necessity of coreceptor ligation: high-affinity peptide-MHC/TCR interaction overcomes lack of CD8 engagement. *J. Immunol.* 171: 4493–4503.
39. Mamalaki, C., T. Norton, Y. Tanaka, A. R. Townsend, P. Chandler, E. Simpson, and D. Kioussis. 1992. Thymic depletion and peripheral activation of class I major histocompatibility complex-restricted T cells by soluble peptide in T-cell receptor transgenic mice. *Proc. Natl. Acad. Sci. USA.* 89: 11342–11346.
40. Long, M., J. Chen, N. Jiang, P. Selvaraj, R. P. McEver, and C. Zhu. 2006. Probabilistic modeling of rosette formation. *Biophys. J.* 91: 352–363.
41. Burshtyn, D. N., and B. H. Barber. 1993. High occupancy binding of antigenic peptides to purified, immunoadsorbed H-2Db β 2m molecules. *J. Immunol.* 151: 3070–3081.
42. MacLachlan, J., A. T. Wotherspoon, R. O. Ansell, and C. J. Brooks. 2000. Cholesterol oxidase: sources, physical properties and analytical applications. *J. Steroid Biochem. Mol. Biol.* 72: 169–195.
43. Cahuzac, N., W. Baum, V. Kirkin, F. Conchonaud, L. Wawrezinieck, D. Marguet, O. Janssen, M. Zornig, and A. O. Hueber. 2006. Fas ligand is localized to membrane rafts, where it displays increased cell death-inducing activity. *Blood* 107: 2384–2391.
44. Xiong, Y., P. Kern, H. Chang, and E. Reinherz. 2001. T Cell Receptor Binding to a pMHCII Ligand Is Kinetically Distinct from and Independent of CD4. *J. Biol. Chem.* 276: 5659–5667.
45. Gao, G. F., B. E. Willcox, J. R. Wyer, J. M. Boulter, C. A. O'Callaghan, K. Maenaka, D. I. Stuart, E. Y. Jones, P. A. Van Der Merwe, J. I. Bell, and B. K. Jakobsen. 2000. Classical and nonclassical class I major histocompatibility complex molecules exhibit subtle conformational differences that affect binding to CD8alphaα. *J. Biol. Chem.* 275: 15232–15238.
46. Wooldridge, L., T. J. Scriba, A. Milicic, B. Laugel, E. Gostick, D. A. Price, R. E. Phillips, and A. K. Sewell. 2006. Anti-coreceptor antibodies profoundly affect staining with peptide-MHC class I and class II tetramers. *Eur. J. Immunol.* 36: 1847–1855.
47. Denkberg, G., C. J. Cohen, and Y. Reiter. 2001. Critical role for CD8 in binding of MHC tetramers to TCR: CD8 antibodies block specific binding of human tumor-specific MHC-peptide tetramers to TCR. *J. Immunol.* 167: 270–276.
48. Schott, E., and H. L. Ploegh. 2002. Mouse MHC class I tetramers that are unable to bind to CD8 reveal the need for CD8 engagement in order to activate naive CD8 T cells. *Eur. J. Immunol.* 32: 3425–3434.
49. Wooldridge, L., S. L. Hutchinson, E. M. Choi, A. Lissina, E. Jones, F. Mirza, P. R. Dunbar, D. A. Price, V. Cerundolo, and A. K. Sewell. 2003. Anti-CD8 antibodies can inhibit or enhance peptide-MHC class I (pMHCI) multimer binding: this is paralleled by their effects on CTL activation and occurs in the absence of an interaction between pMHCI and CD8 on the cell surface. *J. Immunol.* 171: 6650–6660.
50. Fahmy, T. M., J. G. Bieler, and J. P. Schneck. 2002. Probing T cell membrane organization using dimeric MHC-Ig complexes. *J. Immunol. Methods.* 268: 93–106.
51. Norment, A. M., R. D. Salter, P. Parham, V. H. Engelhard, and D. R. Littman. 1988. Cell-cell adhesion mediated by CD8 and MHC class I molecules. *Nature* 336: 79–81.
52. Dustin, M. L. 1997. Adhesive bond dynamics in contacts between T lymphocytes and glass-supported planar bilayers reconstituted with the immunoglobulin-related adhesion molecule CD58. *J. Biol. Chem.* 272: 15782–15788.
53. Dustin, M. L., D. E. Golan, D. M. Zhu, J. M. Miller, W. Meier, E. A. Davies, and P. A. van der Merwe. 1997. Low affinity interaction of human or rat T cell adhesion molecule CD2 with its ligand aligns adhering membranes to achieve high physiological affinity. *J. Biol. Chem.* 272: 30889–30898.
54. Grakoui, A., S. K. Bromley, C. Sumen, M. M. Davis, A. S. Shaw, P. M. Allen, and M. L. Dustin. 1999. The immunological synapse: a molecular machine controlling T cell activation. *Science* 285: 221–227.
55. Long, M., H. Zhao, K. S. Huang, and C. Zhu. 2001. Kinetic measurements of cell surface E-selectin/carbohydrate ligand interactions. *Ann. Biomed. Eng.* 29: 935–946.
56. Zhang, F., W. D. Marcus, N. H. Goyal, P. Selvaraj, T. A. Springer, and C. Zhu. 2005. Two-dimensional kinetics regulation of alphaLβ2-ICAM-1 interaction by conformational changes of the alphaL-inserted domain. *J. Biol. Chem.* 280: 42207–42218.
57. Williams, T. E., P. Selvaraj, and C. Zhu. 2000. Concurrent binding to multiple ligands: kinetic rates of CD16b for membrane-bound IgG1 and IgG2. *Biophys. J.* 79: 1858–1866.
58. Williams, T. E., S. Nagarajan, P. Selvaraj, and C. Zhu. 2000. Concurrent and independent binding of Fcγ receptors IIa and IIIb to surface-bound IgG. *Biophys. J.* 79: 1867–1875.
59. Ding, Y. H., B. M. Baker, D. N. Garboczi, W. E. Biddison, and D. C. Wiley. 1999. Four A6-TCR/peptide/HLA-A2 structures that generate very different T cell signals are nearly identical. *Immunity* 11: 45–56.
60. Devine, L., J. Sun, M. R. Barr, and P. B. Kavathas. 1999. Orientation of the Ig domains of CD8 α β relative to MHC class I. *J. Immunol.* 162: 846–851.